The Astronomical Journal, 152:98 (6pp), 2016 October doi:10.3847/0004-6256/152/4/98

POLARIMETRIC DETECTION OF EXOPLANETS TRANSITING T AND L BROWN DWARFS

Sujan Sengupta
Indian Institute of Astrophysics, Koramangala 2nd Block, Bangalore 560 034, India; sujan@iiap.res.in
Received 2016 April 27; revised 2016 July 6; accepted 2016 July 6; published 2016 October 3

ABSTRACT

While scattering of light by atoms and molecules yields large amounts of polarization at the B-band of both T and L dwarfs, scattering by dust grains in the cloudy atmosphere of L dwarfs gives rise to significant polarization at the far-optical and infrared wavelengths where these objects are much brighter. However, the observable disk-averaged polarization should be zero if the clouds are uniformly distributed and the object is spherically symmetric. Therefore, in order to explain the observed large polarization of several L dwarfs, rotation-induced oblateness or horizontally inhomogeneous cloud distribution in the atmosphere is invoked. On the other hand, when an extra-solar planet of Earth-size or larger transits the brown dwarf along the line of sight, the asymmetry induced during the transit gives rise to a net non-zero, time-dependent polarization. Employing atmospheric models for a range of effective temperature and surface gravity appropriate for T and L dwarfs, I derive the time-dependent polarization profiles of these objects during the transit phase and estimate the peak amplitude of polarization that occurs during the inner contact points of the transit ingress/egress phase. It is found that peak polarization in the range of 0.2%–1.0% at I and J band may arise of cloudy L dwarfs occulted by Earth-size or larger exoplanets. Such an amount of polarization is higher than what can be produced by rotation-induced oblateness of even rapidly rotating L dwarfs. Hence, I suggest that time-resolved imaging polarization could be a potential technique for detecting transiting exoplanets around L dwarfs.

Key words: polarization – radiative transfer – scattering

1. INTRODUCTION

Twenty years after the first confirmed discovery of planets outside the solar system (Wolszczan & Frail 1992; Wolszczan 1994; Mayor & Queloz 1995), about 3000 planets orbiting around stars of different spectral types have been detected. Out of a wide variety of planets with different masses, sizes, and surface temperatures, the recently discovered small and possibly rocky planets that may have surface temperatures appropriate for water to exist in liquid state have become the objects of utmost interest. They have compelled researchers to change their focus to detecting planets that may have favorable environments for harboring life.

Over 80% of the stellar population in the Galaxy consists of red dwarfs and brown dwarfs (Apai 2013). About 15% of the objects in the solar neighborhood are brown dwarfs (Behain & Scholz 2016). Statistical analysis of data obtained by using the *Kepler* space telescope indicates that the occurrence rate of small and potentially rocky planets with radii ranging from 0.5 to 2.0 $R_\oplus$ ($R_\oplus$ is the radius of the Earth) around M dwarf stars is about 0.51 per star (Dressing & Charbonneau 2013; Kopparapu 2013). A good fraction of these rocky planets are believed to be located within the habitable zones of their star. Therefore, a large number of habitable planets are expected in the solar neighborhood and in our Galaxy. However, unlike solar-type stars, M dwarfs are very active as they become fully convective from mid- to late spectral type. They also have intense magnetic fields ranging between 3 and 9 kG (Reid & Hawley 2005). As a consequence, frequent flares and emission of intense X-ray and extreme ultraviolet rays are very common. Therefore, the atmosphere of a planet in the habitable zone of an M dwarf star is unlikely to have favorable conditions for life to survive (Lissauer 2007; Owen & Mohanty 2016; Sengupta 2016). Such a situation strongly motivates the search for habitable planets around brown dwarfs.

Brown dwarfs are believed to be born like stars but fail to become main-sequence stars because they have masses sufficient to ignite deuterium burning but insufficient to enter the hydrogen-burning main sequence. Therefore, they inhabit the realm between the least massive stars and the most massive planets. The source of their observed radiation is the gravitational potential energy during the formation and contraction phases. As the temperature of an individual brown dwarf decreases, the star progressively passes through spectral types ranging from late M through the L, T, and Y sequences. Detailed reviews on the properties of brown dwarfs are given by Chabrier & Baraffe (2000), Basri (2000), Burrows et al. (2001), Kirkpatrick (2005), Luhman (2012), and Marley & Robinson (2015). Synthetic spectra of cloud-free model atmospheres fit well the observed spectra of field T dwarfs later than about type T4 because dust grain condensation takes place well bellow the photosphere and therefore they are not an important opacity source (Stephens et al. 2009). On the other hand, inclusion of condensate clouds of various species such as iron, forsterite (Mg_2SiO_4), and enstatite ($MgSiO_3$) explains the spectra of L dwarfs (Cushing et al. 2008; Marley & Robinson 2015).

Similar to the case of the Sun and cool stars, thermal radiation of both T and L brown dwarfs should be linearly polarized at near-optical wavelengths, e.g., in the B-band due to Rayleigh scattering by atoms and molecules. On the other hand, the presence of dust grains in the visible atmosphere of L dwarfs gives rise to significant amounts of linear polarization in the far-optical and in the infrared regions. However, the net observable polarization would be zero if the object is spherically symmetric and the clouds are distributed uniformly. Linear polarization has been detected in the optical bands from a good number of L dwarfs covering almost the entire range of spectral types L0–L8 (Ménard et al. 2002; Zapatero Osorio et al. 2005, 2011; Tata et al. 2009; Miles-Páez et al. 2013).

Scattering by horizontally homogeneous clouds in the atmosphere of a rotation-induced oblate L dwarf can explain the observed polarization (Sengupta & Krishan 2001; Sengupta 2003; Sengupta & Kwok 2005; Sengupta & Marley 2010). Imaging polarimetric data of L dwarfs shows an increase in the amount of polarization with the increase in spin rotation velocity (Miles-Páez et al. 2013), implying that the asymmetry due to rotation-induced oblateness plays an important role in the linear polarization of fast-rotating dusty L dwarfs. However, in agreement with the analysis of Sengupta & Marley (2009), no polarization in the far-optical and near infrared has been detected from any T dwarf to date.

Apart from the asymmetry that may arise due to rotation-induced oblateness of the stellar disk and/or horizontally inhomogeneous clouds in the atmosphere, asymmetry in the stellar disk can also be produced by a transiting planet that partially blocks the stellar disk. Consequently, the transit of a planet can also give rise to net non-zero disk-integrated polarization. Such transit or occultation polarization of stars of different spectral types has been discussed in detail by a few authors (Carciofi & Magalhaes 2005; Kostogryz et al. 2011; Wiktorowicz & Laughlin 2014).

Giant exoplanets around brown dwarfs have been discovered via direct imaging (Chauvin et al. 2004; Todorov et al. 2010; Gauza et al. 2015; Stone et al. 2016), the radial velocity method (Joergens & Muller 2007), and by using the gravitational microlensing method (Han et al. 2013). Recently a Venus-sized planet has been discovered via microlensing (Udalski et al. 2015). These discoveries clearly imply that formation of exoplanets with sizes ranging from Jovian to sub-Earth is possible around brown dwarfs either through a binary star formation mechanism or through the scale-down core-accretion mechanism of planet formation around a star. Therefore, a large number of exoplanets around brown dwarfs are waiting to be detected (Apai 2013). Discovery of these planets may greatly increase the number of detected exoplanets. In fact, such a realization prompted researchers to propose strategies for detecting habitable planets around brown dwarfs (Caballero & Rebolo 2002; Caballero 2010; Belu et al. 2013). However, as pointed out by Udalski et al. (2015), owing to the limitation of available technology, substantially low mass planetary companions to brown dwarfs can only be discovered at present by using the gravitational microlensing technique. Obviously, the main constraint in detecting Earth-sized planets around brown dwarfs through transit or the radial velocity method is the extreme faintness of these objects.

In this paper, I show that time-resolved image polarimetry can be a potential tool for detecting planets transiting cloudy L dwarfs. Using detailed atmospheric models for cloudy L dwarfs, the scattering polarization is calculated and it is shown that the asymmetry induced by a transiting Earth-sized planet gives rise to significant amount of disk-integrated linear polarization in both I and J bands at the inner contact points of the transit ingress/egress phase which may be detected by existing imaging polarimeters.

In Section 2 I briefly describe the formalism adopted to estimate the time-resolved transit polarization profile of T and L dwarfs. In Section 3, I discuss the results, followed by conclusions in Section 4.

2. METHOD FOR CALCULATING THE TRANSIT POLARIZATION

The net polarization of the L and T dwarfs during the transit is calculated by multiplying the intensity and scattering polarization at each radial point along the disk of the object with the fractional circumference occulted by the projection of the planet over the surface of the primary dwarf. The disk-averaged polarization during the transit phase or the transit polarization is given by Sengupta & Marley (2016), Wiktorowicz & Laughlin (2014), and Carciofi & Magalhaes (2005). Here I use the formalism presented in Sengupta & Marley (2016). Accordingly,

$$p(t) = \frac{1}{F}\int_{r_1}^{r_2} 2\sqrt{\frac{[(1-\mu^2)^{1/2} - r_m(t)]^2 - w^2}{1-\mu^2}} \times I(\mu)p(\mu)\mu d\mu, \quad (1)$$

where t is the time since mid-transit, F is the flux of the unobscured dwarf, $I(\mu)$ and $p(\mu)$ are the specific intensity and polarization, respectively, along μ, $\mu = \cos\theta = \sqrt{1-r^2}$ with θ being the angle between the normal to the surface of the primary and the line of sight and r being the radial points along the disk of the primary, $0 \leqslant r \leqslant 1$, $r_1 = \sqrt{1-[r_m(t)+w]^2}$ and $r_2 = \sqrt{1-[r_m(t)-w]^2}$, $r_m(t)$ is the instantaneous position of the center of the planet and is given by

$$r_m(t) = \left[b^2 + 4\{(1+w)^2 - b^2\}\left(\frac{t}{\tau}\right)^2\right]^{1/2}. \quad (2)$$

In the above expression, the impact parameter b for a circular orbit of radius a is given by $b = a\cos i/R_\star$, where i is the orbital inclination angle of the planet, $R_\star$ is the radius of the L or the T dwarf, and $w = R_P/R_\star$ is the ratio of the planetary radius (R_P) to the radius of the primary. The transit duration τ is given by Scharf (2009)

$$\tau = \frac{P}{\pi}\sin^{-1}\left[\frac{R_\star}{a}\left\{\frac{(1+w)^2 - b^2}{1-\cos^2 i}\right\}^{1/2}\right]. \quad (3)$$

Transit of a planet can occur only if the inclination angle $i \geqslant \cos^{-1}\left(\frac{R_\star + R_P}{a}\right)$.

In order to calculate the specific intensity $I(\mu)$ and scattering polarization $p(\mu)$, I have employed one-dimensional, non-gray, hydrostatic, and radiative-convective atmospheric models for a range of effective temperature $T_{\rm eff}$ and surface gravities g appropriate for T and L dwarfs (Ackerman & Marley 2001; Marley et al. 2002; Freedman et al. 2008; Saumon & Marley 2008). For T dwarfs, a cloudless model atmosphere generally reproduces the spectra of most T dwarfs with $T_{\rm eff} < 1200$–1300 K (Stephens et al. 2009). In the present work, I consider cloudless models for T dwarfs appropriate for spectral types later than about T3 (Stephens et al. 2009). However, condensates are included in the chemical equilibrium calculation (Freedman et al. 2008). For T dwarfs, I choose models with $T_{\rm eff} = 1300$, 1100, 900, and 700 K for a fixed value of $g = 1000\,{\rm m\,s^{-2}}$.

For the relatively hotter L dwarfs, a spatially uniform dust cloud is included. The efficiency of sedimentation of cloud particles in the atmospheric models is controlled through a

scaling factor $f_{\rm sed}$. In the present work I adopt $f_{\rm sed} = 2.0$ (Cushing et al. 2008; Stephens et al. 2009). For L dwarfs, I choose models with $T_{\rm eff} = 1400$, 1600, 1800, 2000 and 2200 K for a fixed surface gravity $g = 1000\,{\rm m\,s^{-2}}$. A few representative cases for $g = 300\,{\rm m\,s^{-2}}$ are also presented for comparison. The atmosphere models employed here fit reasonably well the spectra and photometry of a large number of T and L dwarfs at a wide range of wavelengths covering near-optical to mid-infrared regions (Marley & Robinson 2015).

The gas and dust opacity, the temperature-pressure profile, and the dust scattering asymmetry function averaged over each atmospheric pressure level are computed using the atmospheric code. In order to calculate the two non-zero Stokes parameters I and Q in a locally plane-parallel medium, these input data are used in a multiple scattering polarization code that solves the radiative transfer equations in vector form. It is worth mentioning that for linear polarization of an axially symmetric radiation field, the other two Stokes parameters, U and V, are zero. For the cloudy L dwarfs, the angular distribution of the photons before and after scattering is calculated by using a combined Henyey–Greenstein–Rayleigh phase matrix (Liu & Weng 2006), while for cloudless T dwarfs, a Rayleigh phase matrix is sufficient to describe the scattering by atoms and molecules (Chandrasekhar 1960, p. 79). The detailed formalisms as well as the numerical methods for calculating the angle-dependent total and polarized intensity I and Q are described in Sengupta & Marley (2009). In fact, in order to calculate the transit or occultation polarization profiles presented here, I have used the same values of $I(\mu)$ and $p(\mu)$ that are used in Sengupta & Marley (2009) for T dwarfs and in Sengupta & Marley (2010) for L dwarfs.

If the reflected light of the planet is polarized due to the presence of clouds in the planetary atmosphere, a small amount of phase-dependent polarization may arise at far-optical and infrared wavelenghts. However, because of very small planet-to-dwarf flux ratio, the amount of such a polarization should be insignificant as compared to the polarization of the brown dwarf (Seager et al. 2000; Sengupta & Maiti 2006; Bott et al. 2016). Hence, we ignore any contribution from the planet to the net polarization of the system.

Although the atmospheric code derives a different radius for the brown dwarf for a different surface gravity and effective temperature, in order to derive the transit duration of a planet with a fixed orbital separation $a = 0.01$ au, I assume the radius of the brown dwarf to be $1R_{\rm J}$ where $R_{\rm J}$ is the radius of Jupiter. However, for a given surface gravity, this does not alter the transit duration significantly. For example, with a fixed surface gravity $g = 1000\,{\rm m\,s^{-2}}$, the transit duration of an Earth-sized planet orbiting a brown dwarf with radius 1.5 $R_{\rm J}$ is 0.72 hr when the orbital inclination angle is 90° while the transit duration of an Earth-sized planet orbiting the primary with radius $1R_{\rm J}$ is 0.74 hr. It must be emphasized here that this is just a representative case. The amount of polarization originating due to transit is not affected by the orbital distance or period of the planet. The orbital separation and the orbital period determine the transit duration which provides the interval between the two successive amplitudes of polarization that occur at the inner contact points of the transit ingress/egress phase as depicted in Figure 1. The amount of transit polarization depends on the ratio between the radii of the planet and the L or T dwarf.

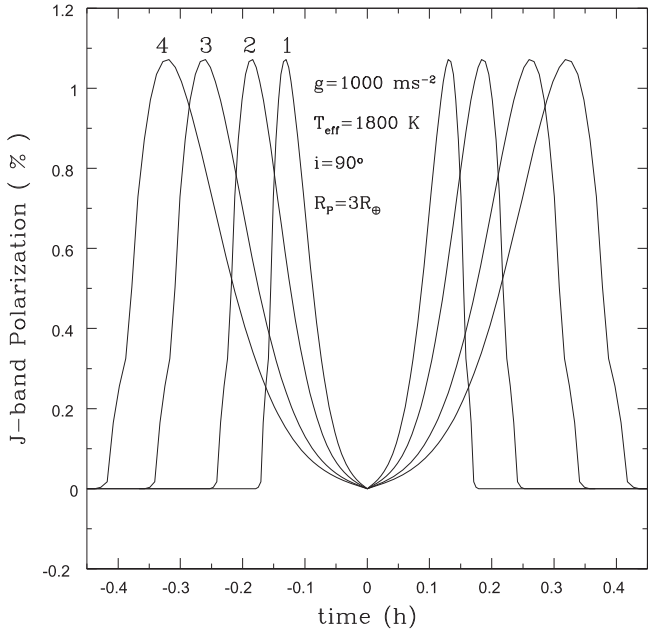

Figure 1. Transit polarization of an L dwarf by a planet with different orbital separations a. The labels represent the polarization profile for different values of a in au. (1) $a = 0.005$, (2) $a = 0.01$, (3) $a = 0.1$, and (4) $a = 0.2$. A Jupiter-sized L dwarf is assumed.

3. RESULTS AND DISCUSSIONS

The center-to-limb variation in the polarization across any stellar disk arises due to the scattering albedo which is determined by the contribution of scattering opacity to the total opacity in the atmosphere (Harrington 1969). The polarization is zero at the center ($\mu = 1$) of the stellar disk and is maximum at the limb ($\mu = 0$). Linear polarization in cool stars arises by scattering of light with atoms and molecules and the maximum amount of polarization that occurs at the stellar limb is usually very small. Polarization for solar-type stars varies from a few times 10^{-4} near the limb to a few times 10^{-6} near the center at near-optical (B-band) wavelengths (Fluri & Stenflo 1999). At longer wavelengths, the polarization is extremely small. The scattering polarization of cloudless T dwarfs does not differ significantly from that of a cool star but large amounts of polarization in longer wavelengths arise due to dust scattering in cloudy L dwarfs.

As mentioned earlier, in the absence of clouds in the visible atmosphere, the polarization of T dwarfs arises due to Rayleigh scattering by atoms and molecules. Therefore the largest amount of polarization arises at shorter wavelengths. Figure 2 presents the B-band transit or occultation polarization of T dwarfs with different effective temperatures. For a fixed surface gravity, the gas density increases with the decrease in $T_{\rm eff}$ and hence the scattering probability increases, yielding higher polarization. It is worth mentioning that the amount of scattering polarization at different angular points is determined by the atmospheric models invoked.

The double-peaked polarization profile, a general feature of transit polarization of any object, arises because of the fact that the maximum polarization occurs near the inner contact points of transit ingress/egress phases. For central transit, i.e., when the inclination angle $i = 90°$, the projected position of the center of the planet coincides with the center of the star during mid-transit. This gives rise to a symmetry to the projected

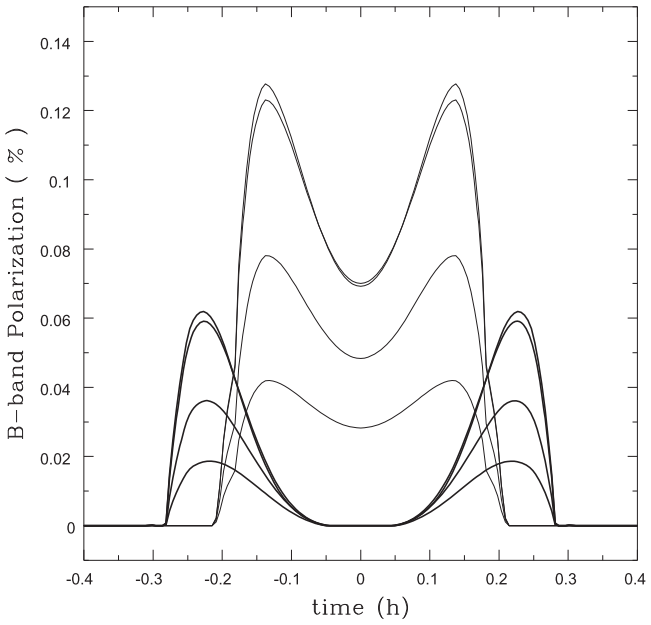

Figure 2. Disk-integrated B-band polarization of T dwarfs during the transit of an exoplanet. From top to bottom, the thick and thin solid lines represent T dwarf models with $T_{\rm eff}$ = 700, 900, 1100, and 1300 K, respectively. The thick solid lines represent models for an Earth-sized transiting planet with a 90° orbital inclination angle and the thin solid lines represent models for a transiting exoplanet with radius of $3R_{\oplus}$ and an inclination angle of 89°. For all cases, the radius of the T dwarf is set to $1R_{\rm J}$ and $g = 1000\ {\rm m\ s^{-2}}$. The orbital distance of the exoplanet is 0.01 au.

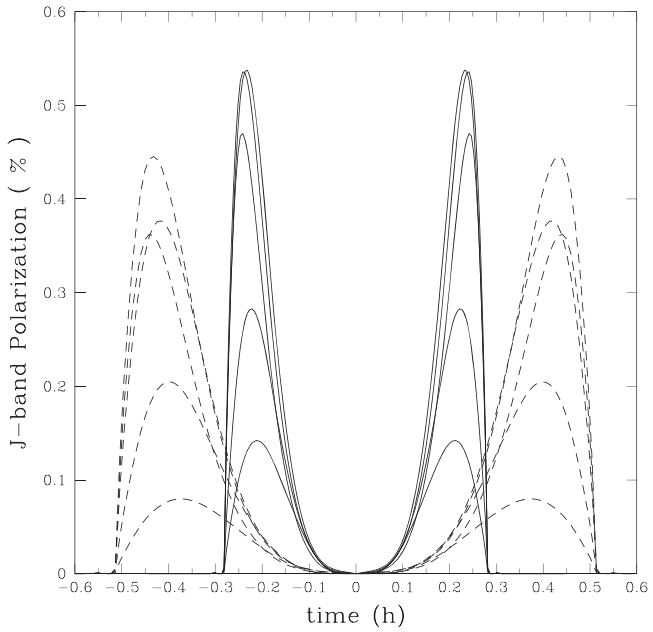

Figure 3. Disk-integrated J-band polarization of a cloudy L dwarf during the transit of an Earth-sized planet with an orbital inclination angle of $i = 90°$ and an orbital distance of $a = 0.01$ au. Solid lines represent an L dwarf with a surface gravity of $g = 1000\ {\rm m\ s^{-2}}$ and dashed lines represent an L dwarf with $g = 300\ {\rm m\ s^{-2}}$. From top to bottom the lines represent L dwarfs with $T_{\rm eff}$ = 1600, 1800, 1400, 2000, and 2200 K, respectively.

stellar disk. Hence the disk-integrated polarization for central transit is zero during mid-transit. Owing to an increase in asymmetry to the stellar disk, the polarization increases as the planet moves from the center ($t = 0$) to the limb ($t = \pm\tau/2$) of the stellar disk. However, when the eclipse is off-center, i.e., when $i \leqslant 90°$, the polarization is non-zero during the whole transit epoch including the mid-transit time. Nevertheless, the peak polarization is independent of the orbital inclination angle but depends on the ratio of the planetary to stellar radii.

As presented in Figure 2, for an Earth-sized transiting planet, the B-band peak polarization at the inner contact points of transit ingress/egress phase is 0.06% for T dwarfs with $T_{\rm eff} = 700$ K. The peak polarization becomes about 0.12% when the size of the transiting planet is three times the size of the Earth. The asymmetry in the stellar disk increases with the increase in the ratio between the planetary and stellar radii and hence the disk-integrated polarization increases. The transit duration depends on the size of both the primary and the planet, on the orbital distance of the planet from the star or brown dwarf, on the orbital period, and on the planetary orbital inclination angle. Therefore, for a given orbital distance, the peak polarization occurs at different times for different size ratios and inclination angles.

The amount of transit polarization of a T dwarf is maximum at B band and the peak polarization is very small, between 0.02% and 0.06%, for an Earth-sized transiting planet. Since the object is also faint at near-optical, detecting such low polarization could be challenging. It is worth mentioning here that a B-band polarimetric observation of brown dwarfs has not been reported to date and no polarization is detected for any T dwarf at longer wavelengths (Jensen–Clem et al. 2016).

On the other hand, formation of dust grains in the cloudy atmosphere of L dwarfs provides an additional scattering opacity to the gas opacity. The thermal radiation of the cloudy L dwarfs is polarized by dust scattering giving rise to large values of limb polarization in the far-optical and infrared wavelengths. Figure 3 presents the J-band transit polarization of L dwarfs. Although the overall feature of the transit polarization profile remains the same as that of T dwarfs at B band, the degree of polarization increases by several times at J band. As demonstrated by Sengupta & Marley (2010) and Marley & Sengupta (2011), the degree of polarization of cloudy L dwarfs and self-luminous exoplanets depends on the effective temperature and the surface gravity of the objects. The scattering opacity is determined by a balance between the downward transport by sedimentation and upward turbulent diffusion of condensates and gas and hence the polarization varies with different effective temperatures and surface gravities. Figure 3 shows that L dwarfs of mid-spectral type corresponding to $T_{\rm eff} = 1600$–1800 K produce the largest amount of polarization at the inner contact points of transit ingress/egress phase when the surface gravity $g = 1000\ {\rm m\ s^{-2}}$. Polarization reduces with the decrease in surface gravity and effective temperature. At the same time, for a given surface gravity, polarization reduces when the effective temperature of the object rises above 1800 K. An increase in temperature causes the cloud base to shift upward, yielding a smaller column of dust grains in the observed atmosphere and hence the polarization decreases with the increase in effective temperature.

Although the scattering polarization is sensitive to the effective temperature and the surface gravity, the amount of transit polarization strongly depends on the asymmetry in the stellar disk produced during the transit phase. This asymmetry is governed by the size of the transiting planet as compared to the size of the L dwarf. Figure 4 presents the transit polarization at I and J bands of an L dwarf with fixed surface

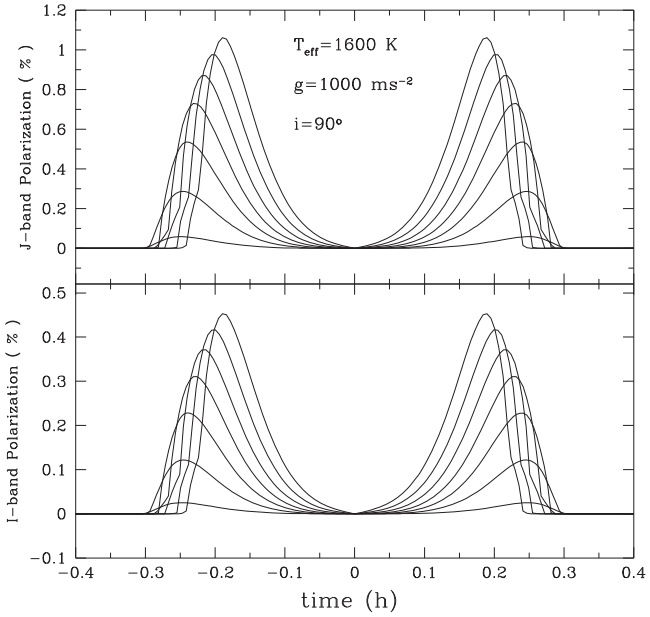

Figure 4. Disk-integrated J- and I-band polarization of an L dwarf with $T_{\rm eff} = 1600$ K and $g = 1000\,{\rm m\,s^{-2}}$ during the transit of exoplanets with different sizes but with a fixed orbital inclination angle $i = 90^\circ$ and orbital distance $a = 0.01$ au. In both panels, the solid lines from top to bottom represent polarization by transiting exoplanet of radius 0.1, 0.5, 1.0, 1.5, 2.0, 2.5, and 3.0 $R_\oplus$, respectively, where $R_\oplus$ is the radius of the Earth.

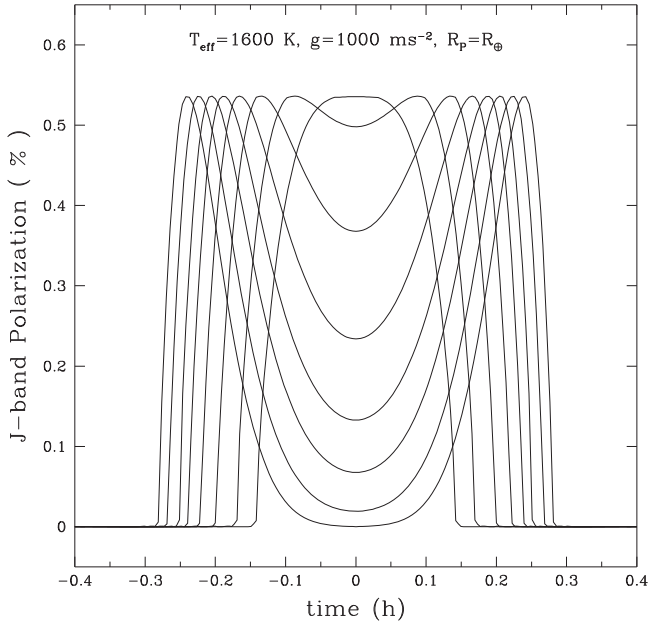

Figure 5. Disk-integrated J-band polarization of an L dwarf with $T_{\rm eff} = 1600$ K and $g = 1000\,{\rm m\,s^{-2}}$ during the transit of an Earth-sized planet orbiting at a distance of 0.01 au but with different orbital inclination angles. From bottom to top at 0 h, the solid lines represent models with $i = 90.0$, 89.3, 89.0, 88.8, 88.6, 88.4, 88.2, and 88.0, respectively.

gravity and effective temperature but for different sizes of the transiting planet. As the asymmetry increases with the increase in the size of the transiting planet, the amount of polarization at the inner contact points of the ingress/egress phases increases linearly. Figure 4 also indicates that the amount of polarization in J band is higher than that in I band. In fact, the peak amplitude of polarization in J band is almost double that in I band. The adopted cloud model, e.g., the size distribution, the number density of the dust grains, as well as the location of the cloud base and deck dictates the amount of polarization at different wavelengths.

As mentioned before, the orbital inclination angle of the transiting planet does not determine the amount of polarization at the inner contact points of the transit ingress/egress phase but affects the time interval between the two successive peaks of polarization. Figure 5 shows the J-band transit polarization due to a transiting planet having different orbital inclination angles. As the inclination angle decreases from its maximum value of 90°, the transit path of the planet shifts toward the edge of the primary, shortening the transit period. The amount of polarization at mid-transit ($t = 0$) increases with the decrease in inclination angle. As the distance between the inner contact points of the ingress and the egress phases shorten, the time interval between the occurrence of the two polarization peaks reduces, and subsequently, the two peaks merge into one central peak when the inclination angle attains its minimum value beyond which a full transit is not possible. This is consistent with the results presented by Carciofi & Magalhaes (2005) for solar-type stars. A partial transit, however, reduces the degree of disk-integrated polarization.

Brown dwarfs are fast rotators and rotation causes departure from sphericity. The asymmetry induced by rotation can yield a net non-zero disk-integrated polarization (Sengupta & Krishan 2001). However, as shown by Sengupta & Marley (2010), the net degree of linear polarization in J band of a brown dwarf with surface gravity $g = 1000\,{\rm m\,s^{-2}}$ yields as little as 0.06% polarization even if the projected rotational velocity is about $50\,{\rm km\,s^{-1}}$. In order to produce 0.2% polarization, a brown dwarf needs to have an oblateness greater than 0.2. For a surface gravity of $1000\,{\rm m\,s^{-2}}$, this can never be achieved as the rotation velocity cannot exceed the breaking velocity. Therefore, the amount of polarization at the inner contact points of the transit ingress/egress phases clearly implies that the asymmetry produced by an Earth-sized transiting planet is higher than that caused by rotation-induced oblateness of even fast-rotating brown dwarfs. Although rotation-induced oblateness explains the observed I-band polarization of many L dwarfs, the required asymmetry needs a surface gravity much lower than $1000\,{\rm m\,s^{-2}}$ (Sengupta & Marley 2010). The synthetic spectra of brown dwarfs poorly constrain the surface gravity—within a wide range of 300–3000 $\rm m\,s^{-2}$. But some L dwarfs show such a large polarization that it can be explained only if the spin rotation velocity is extremely high even if the surface gravity is taken to be $300\,{\rm m\,s^{-2}}$. For example, the observed degree of polarization for 2MASS J2158−1550 (L4.0) and 2MASS J1807+5015 (L1.5) is 1.38% and 0.7%, respectively, and so a spin rotation velocity of more than $100\,{\rm km\,s^{-1}}$ is required to explain such high polarization. None of these L dwarfs showed optical variability, thus this rules out high inhomogeneity in atmospheric cloud distribution. On the other hand, I-band polarization as high as 2.45% was observed from 2MASS J2244+2043 (L6.5). This object is found to be variable at 4.5 μm (Morales-Calderón et al. 2006). However, it is unlikely that cloud inhomogeneity can account for such a large amount of polarization. As pointed out by Sengupta & Marley (2010), quite a few L dwarfs that are optically variable do not show polarization, implying cloud inhomogeneity that may be responsible for variability cannot contribute significantly to yielding detectable polarization. Transit by a Neptunian planet may explain such high polarization and

time-resolved imaging polarimetry may verify such a possibility. If the high polarization is caused by rotation-induced oblateness, the amount of polarization should remain time-independent. On the other hand, cloud inhomogeneity should cause variable polarization. In both cases, the contribution due to rotation-induced oblateness or cloud inhomogeneity may be estimated when the primary source is out of the transit phase.

4. CONCLUSIONS

Assuming the transit of an exoplanet around cloudy L dwarfs and cloudless T dwarfs, I have presented the transit polarization profiles of brown dwarfs and estimated the peak polarization at the inner contact points of the transit ingress/egress phases for a large number of model atmospheres and planetary radii. For this purpose, the atmospheric models that fit the observed spectra of T and L dwarfs are employed. The B-band linear polarization due to scattering by atoms and molecules in the atmosphere of T dwarfs and I- and J-band linear polarization due to scattering by dust grains in the atmosphere of L dwarfs are calculated numerically. The present investigation implies that a significant amount of transit polarization may arise in both I and J bands of a cloudy L dwarf if an Earth-sized or larger planet transits it, giving rise to asymmetry in the stellar disk. However, the transit polarization of the cloudless T dwarfs is significant only in the B band where these objects are extremely faint and hence detection of the polarization signal is difficult. Therefore, it is suggested that time-resolved imaging polarimetry should be a potential technique to detect small rocky planets around L dwarfs.

Our model estimations imply that for L dwarfs with spectral types ranging from L3 to L7, the peak polarization at the inner contact points of the transit ingress/egress phases should be 0.5%–1.0% in the J band and 0.2%–0.5% in the I band for transiting planets of size 1–3$R_{\oplus}$. Such an amount of polarization can easily be detected by several existing facilities including FORS1 on board VLT and LIRIS on board WHT.

I thank the reviewer for a critical reading of the manuscript and for providing many useful suggestions.

REFERENCES

Ackerman, A., & Marley, M. S. 2001, ApJ, 556, 872
Apai, D. 2013, AN, 334, 57
Basri, G. 2000, ARA&A, 38, 485
Behain, G., & Scholz, R.-D. 2016, A&A, 589, 26
Belu, A. R., Selsis, F., Raymond, S. N., et al. 2013, ApJ, 768, 125
Bott, K., Bailey, J., Kedziora-Chudezer, L., et al. 2016, MNRAS, 459, L109
Burrows, A., Hubbard, W. B., Lunine, J. I., & Liebert, J. 2001, RvMP, 73, 719
Caballero, J. A. 2010, in Astrophysics and Space Science Proc., Highlights of Spanish Astrophysics V, ed. J. M. Diego et al. (Berlin: Springer), 79
Caballero, J. A., & Rebolo, R. 2002, in First Eddington Workshop on Stellar Structure and Habitable Planet Finding, ed. F. Favata, I. W. Roxburgh, & D. Galadí Enríquez, (Noordwijk: ESA), 261 ESA SP-485
Carciofi, A. C., & Magalhaes, A. M. 2005, ApJ, 635, 570
Chabrier, G., & Baraffe, I. 2000, ARA&A, 38, 337
Chandrasekhar, S. 1960, Radiative Transfer (New York, NY: Dover)
Chauvin, G., Lagrange, A.-M., Dumas, C., et al. 2004, A&A, 425, L29
Cushing, M. C., Marley, M. S., Saumon, D., et al. 2008, ApJ, 678, 1372
Dressing, C. D., & Charbonneau, D. 2013, ApJ, 767, 95
Fluri, D. M., & Stenflo, J. O. 1999, A&A, 341, 902
Freedman, R. S., Marley, M. S., & Katharina, L. 2008, ApJS, 174, 504
Gauza, B., Béjar, V. J. S., Pérez-Garrido, A., et al. 2015, ApJ, 804, 96
Han, C., Jung, Y. K., Udalski, A., et al. 2013, ApJ, 778, 38
Harrington, J. P. 1969, ApL, 3, 165
Jensen-Clem, R., Millar-Blanchaer, M., Mawet, D., et al. 2016, ApJ, 820, 111
Joergens, V., & Muller, A. 2007, ApJL, 666, L113
Kirkpatrick, J. D. 2005, ARA&A, 43, 195
Kopparapu, R. K. 2013, ApJL, 767, L8
Kostogryz, N. M., Yakobchuk, T. M., Morozhenko, O. V., & VidMachenko, A. P. 2011, MNRAS, 415, 695
Lissauer, J. J. 2007, ApJL, 660, L149
Liu, Q., & Weng, F. 2006, ApOpt, 45, 7475
Luhman, K. L. 2012, ARA&A, 50, 65
Marley, M. S., & Robinson, T. D. 2015, ARA&A, 53, 279
Marley, M. S., & Sengupta, S. 2011, MNRAS, 417, 2874
Marley, M. S., Seager, S., Saumon, D., et al. 2002, ApJ, 568, 335
Mayor, M., & Queloz, D. 1995, Natur, 378, 355
Ménard, F., Delfosse, X., & Monin, J.-L. 2002, A&A, 396, L35
Miles-Páez, P. A., Zapatero Osorio, M. R., Pall, E., & Peña Ramirez, K. 2013, A&A, 556, 125
Morales-Calderón, M., Stauffer, J. R., Kirkpatrick, J. D., et al. 2006, ApJ, 653, 1454
Owen, J. E., & Mohanty, S. 2016, MNRAS, 459, 4088
Reid, I. N., & Hawley, S. L. 2005, New Light on Dark Stars Red Dwarfs, Low-Mass Stars, Brown Stars (Chichester: Praxis Publishing Ltd)
Saumon, D., & Marley, M. S. 2008, ApJ, 689, 1327
Scharf, C. A. 2009, Extrasolar Planets and Astrobilogy (Sausalito, California: Univ. Science Books) Chapter 9
Seager, S., Whitney, B. A., & Sasselov, D. 2000, ApJ, 540, 504
Sengupta, S. 2003, ApJL, 585, L155
Sengupta, S. 2016, A&A, 37, 11
Sengupta, S., & Krishan, V. 2001, ApJL, 561, L123
Sengupta, S., & Kwok, S. 2005, ApJ, 625, 996
Sengupta, S., & Maiti, M. 2006, ApJ, 639, 1147
Sengupta, S., & Marley, M. S. 2009, ApJ, 707, 716
Sengupta, S., & Marley, M. S. 2010, ApJL, 722, L142
Sengupta, S., & Marley, M. S. 2016, ApJ, 824, 76
Stephens, D. C., Leggett, S. K., Cushing, M. C., et al. 2009, ApJ, 702, 154
Stone, J. M., Skemer, A. J., Kratter, K. M., et al. 2016, ApJL, 818, L12
Tata, R., Martin, E. L., Sengupta, S., et al. 2009, A&A, 508, 1423
Todorov, K., Luhman, K. L., & McLeod, K. K. 2010, ApJL, 714, L84
Udalski, A., Jung, Y. K., Han, C., et al. 2015, ApJ, 812, 47
Wiktorowicz, S. J., & Laughlin, G. P. 2014, ApJ, 795, 12
Wolszczan, A. 1994, Sci, 264, 538
Wolszczan, A., & Frail, D. A. 1992, Natur, 355, 145
Zapatero Osorio, M. R., Béjar, V. J. S., Goldman, B., et al. 2011, ApJ, 740, 4
Zapatero Osorio, M. R., Caballero, J. A., & Béjar, V. J. S. 2005, ApJ, 621, 445